REPORT DOCUMENTATION PAGE

Form Approved OMB NO. 0704-0188

1. REPORT DATE (DD-MM-YYYY)	2. REPORT TYPE	3. DATES COVERED (From - To)
02-10-2014	Final Report	15-Nov-2009 - 30-Jun-2014

4. TITLE AND SUBTITLE
Final Report: Wide-bandgap III-Nitride based Second Harmonic Generation

5a. CONTRACT NUMBER

5b. GRANT NUMBER
W911NF-04-D-0003

5c. PROGRAM ELEMENT NUMBER
611102

6. AUTHORS
Michael Gerhold, Marc Hoffmann, Ramon Collazo, Zlatko SItar

5d. PROJECT NUMBER

5e. TASK NUMBER

5f. WORK UNIT NUMBER

7. PERFORMING ORGANIZATION NAMES AND ADDRESSES
North Carolina State University
2901 Sullivan Drive
Suite 240, Campus Bx 7514
Raleigh, NC 27695 -7003

8. PERFORMING ORGANIZATION REPORT NUMBER

9. SPONSORING/MONITORING AGENCY NAME(S) AND ADDRESS (ES)
U.S. Army Research Office
P.O. Box 12211
Research Triangle Park, NC 27709-2211

10. SPONSOR/MONITOR'S ACRONYM(S)
ARO

11. SPONSOR/MONITOR'S REPORT NUMBER(S)
57365-EL-SR.6

12. DISTRIBUTION AVAILIBILITY STATEMENT
Approved for Public Release; Distribution Unlimited

13. SUPPLEMENTARY NOTES
The views, opinions and/or findings contained in this report are those of the author(s) and should not contrued as an official Department of the Army position, policy or decision, unless so designated by other documentation.

14. ABSTRACT
It was demonstrated that GaN, AlGaN and AlN lateral polar structures can be manufactured that are promising for second harmonic generation using quasi phase matching. In GaN LPS the growth rate of the polar domains significantly depends on the applied Ga supersaturation. AlN LPS can be manufactured easily with no growth rate difference between polar domains. In AlGaN LPS, it could be observed that high Ga composition in the AlxGa1-xN LPS leads to a height difference of the domains towards the III-polarity. It has been suggested that this is strongly influenced by the Ga supersaturation, as observed in GaN LPS. Nevertheless, the fabricated AlxGa1-xN LPSs are

15. SUBJECT TERMS
nonlinear optics, gallium nitride, quasi-phase matching, lateral polar structures

16. SECURITY CLASSIFICATION OF:			17. LIMITATION OF ABSTRACT	15. NUMBER OF PAGES	19a. NAME OF RESPONSIBLE PERSON
a. REPORT	b. ABSTRACT	c. THIS PAGE			Michael Gerhold
UU	UU	UU	UU		19b. TELEPHONE NUMBER 919-549-4357

Report Title

Final Report: Wide-bandgap III-Nitride based Second Harmonic Generation

ABSTRACT

It was demonstrated that GaN, AlGaN and AlN lateral polar structures can be manufactured that are promising for second harmonic generation using quasi phase matching. In GaN LPS the growth rate of the polar domains significantly depends on the applied Ga supersaturation. AlN LPS can be manufactured easily with no growth rate difference between polar domains. In AlGaN LPS, it could be observed that high Ga composition in the AlxGa1-xN LPS leads to a height difference of the domains towards the III-polarity. It has been suggested that this is strongly influenced by the Ga supersaturation, as observed in GaN LPS. Nevertheless, the fabricated AlxGa1-xN LPSs are promising to be used for QPM waveguides as an alter-native to achieve deep UV light-emitters. GaN and AlN waveguides can be used to realize modal-dispersion phase matching enabling SHG.

Enter List of papers submitted or published that acknowledge ARO support from the start of the project to the date of this printing. List the papers, including journal references, in the following categories:

(a) Papers published in peer-reviewed journals (N/A for none)

Received		Paper
10/09/2013	1.00	Jinqiao Xie, Seiji Mita, Zachary Bryan, Wei Guo, Lindsay Hussey, Baxter Moody, Raoul Schlesser, Ronny Kirste, Michael Gerhold, Ramon Collazo, Zlatko Sitar. Lasing and longitudinal cavity modes in photo-pumped deep ultraviolet AlGaN heterostructures, Appl. Phys. Lett., (04 2013): 171102. doi:
10/09/2013	2.00	Ronny Kirste, Seiji Mita, Lindsay Hussey, Marc Hoffmann, Wei Guo, Isaac Bryan, Zachary Bryan, James Tweedie, Jinqiao Xie, Michael Gerhold, Ramon Collazo, Zlatko Sitar. Polarity Control and growth of lateral polarity structures in AlN, Appl. Phys. Lett., (05 2013): 181913. doi:
10/09/2013	3.00	Martin Rigler, Marko Zgonik, Marc Hoffmann, Ronny Kirste, Milena Bobea, Ramon Collazo, Zlatko Sitar, Seiji Mita, Michael Gerhold. Refractive index of III-metal-polar and N-polar AlGaN waveguides grown by metal organic chemical vapor deposition, Appl. Phys. Lett., (06 2013): 221106. doi:
TOTAL:		**3**

Number of Papers published in peer-reviewed journals:

(b) Papers published in non-peer-reviewed journals (N/A for none)

Received		Paper
TOTAL:		

Number of Papers published in non peer-reviewed journals:

(c) Presentations

Number of Presentations: 0.00

Non Peer-Reviewed Conference Proceeding publications (other than abstracts):

Received	Paper

TOTAL:

Number of Non Peer-Reviewed Conference Proceeding publications (other than abstracts):

Peer-Reviewed Conference Proceeding publications (other than abstracts):

Received	Paper	
10/10/2013	5.00	Marc Hoffmann, Michael Gerhold, Ronny Kirste, Anthony Rice, Christer-Rajiv Akouala, Jinqiao Xie, Seiji Mita, Ramon Collazo, Zlatko Sitar. Fabrication and Characterization of Lateral Polar GaN Structures for Second Harmonic Generation, SPIE Photonics West (2013): Quantum Sensing and Nanophotonics. 04-FEB-13, . : ,

TOTAL: **1**

Number of Peer-Reviewed Conference Proceeding publications (other than abstracts):

(d) Manuscripts

Received	Paper

TOTAL:

Number of Manuscripts:

Books

Received	Book

TOTAL:

Received	Book Chapter

TOTAL:

Patents Submitted

Patents Awarded

Awards

M. Rigler, et al, 2014 Best student paper award at the European Materials Research Society meeting for UV Second Harmonic Generation in Aluminum Gallium Nitride semiconductors

M. Hoffmann, et al, 2013 Best student paper award at the European Materials Research Society meeting for Point defect reduction via UV illumination during growth of Aluminum Gallium Nitride Semiconductors

Graduate Students

NAME	PERCENT_SUPPORTED	Discipline
Marc Hoffmann	1.00	
FTE Equivalent:	**1.00**	
Total Number:	**1**	

Names of Post Doctorates

NAME	PERCENT_SUPPORTED
FTE Equivalent:	
Total Number:	

Names of Faculty Supported

NAME	PERCENT_SUPPORTED	National Academy Member
Zlatko Sitar	0.01	
FTE Equivalent:	**0.01**	
Total Number:	**1**	

Names of Under Graduate students supported

NAME	PERCENT_SUPPORTED
FTE Equivalent:	
Total Number:	

Student Metrics

This section only applies to graduating undergraduates supported by this agreement in this reporting period

The number of undergraduates funded by this agreement who graduated during this period:	0.00
The number of undergraduates funded by this agreement who graduated during this period with a degree in science, mathematics, engineering, or technology fields:.....	0.00
The number of undergraduates funded by your agreement who graduated during this period and will continue to pursue a graduate or Ph.D. degree in science, mathematics, engineering, or technology fields:.....	0.00
Number of graduating undergraduates who achieved a 3.5 GPA to 4.0 (4.0 max scale):.....	0.00
Number of graduating undergraduates funded by a DoD funded Center of Excellence grant for Education, Research and Engineering:.....	0.00
The number of undergraduates funded by your agreement who graduated during this period and intend to work for the Department of Defense	0.00
The number of undergraduates funded by your agreement who graduated during this period and will receive scholarships or fellowships for further studies in science, mathematics, engineering or technology fields:	0.00

Names of Personnel receiving masters degrees

NAME
Total Number:

Names of personnel receiving PHDs

NAME
Marc Hoffmann
Total Number: 1

Names of other research staff

NAME	PERCENT_SUPPORTED
FTE Equivalent:	
Total Number:	

Sub Contractors (DD882)

Inventions (DD882)

Scientific Progress

See attachment

Technology Transfer

Results of the research have been socialized to the III-Nitride Optoelectronics Center of Excellence (ARL SEDD) and to the 2013 ARO Staff Research Symposium and at numerous technical symposium including the 2013 International Conference on Nitrides (ICNS), Washington, D. C. and the 2014 European MRS.

Final report:

“Wide-bandgap III-Nitride based Second Harmonic Generation”

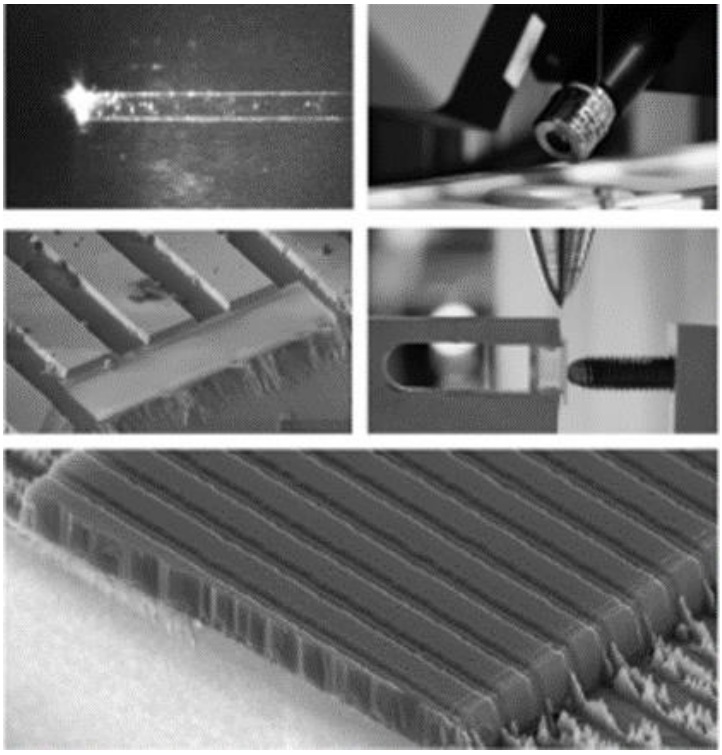

Michael Gerhold

Marc Hoffmann

Ramon Collazo

Zlatko Sitar

Contents

1. Introduction

Quadratic nonlinear optical materials like GaN, AlN and their alloys allow conversion and extension of the wavelengths of coherent light sources via second-harmonic generation (SHG). Therefore, AlGaN crystalline films grown with MOCVD can be used to convert a laser beam to coherent light with photons of double energy. Because of their transparency in UV and two possible polar orientations along the c-axis, III-nitrides can be efficient harmonic generators. Quasi-phase matching (or QPM) is required in AlGaN to exploit the NLO properties of the material since there is no sufficient birefringence to sustain efficient SHG. In the case of AlGaN, with a non-centrosymmetric crystal structure, this is achieved by periodically inverting the direction of the optical axis (here it is the c-axis) of the material, growing periodic structures of III- and N-polar with the desired domain length (determined by photolithographic patterning – usually several microns).

The main research highlights in this report are based on the breakthrough of demonstrating AlGaN-based quasi-phase matching waveguides with similar thicknesses for both polar domains. Two main challenges are addressed in this report: (1) the demonstration of periodic lateral polarity control in $Al_xGa_{1-x}N$ alloys, and (2) the development of the basic understanding of non-linear optical characteristics of these structures. As described in the highlights, in part of this work we have demonstrated the first periodically patterned AlN film that will serve as the quasi-based matching waveguide. In addition, the optical properties of AlN and AlGaN high quality thin films and waveguides were characterized as needed for the designed of the quasi-phased matched structures. In the following, a summary describing the results from these achievements will be presented.

2. Fabrication process of $Al_xGa_{1-x}N$ LPS

The fabrication of AlGaN LPS is a 4 step process. The first step consists of the growth of a 20 nm thick low temperature-(LT-) AlN film at 650°C on c-sapphire. The nucleation layer was used to assure the III-polarity for AlGaN. Prior to the growth of nucleation layer, the sapphire substrate is exposed to H_2-etching for 7 min, followed by NH_3-annealing for 4 min. The H_2-etching is needed to remove unwanted contaminants and create a suitable step-and-terrace sapphire surface morphology. The NH_3-annealing is used to modify the sapphire surface and form a thin AlN layer to control the polarity. This first step is always the same for all fabricated AlGaN LPS. Fig. 1 shows the fabrication process for a GaN LPS.

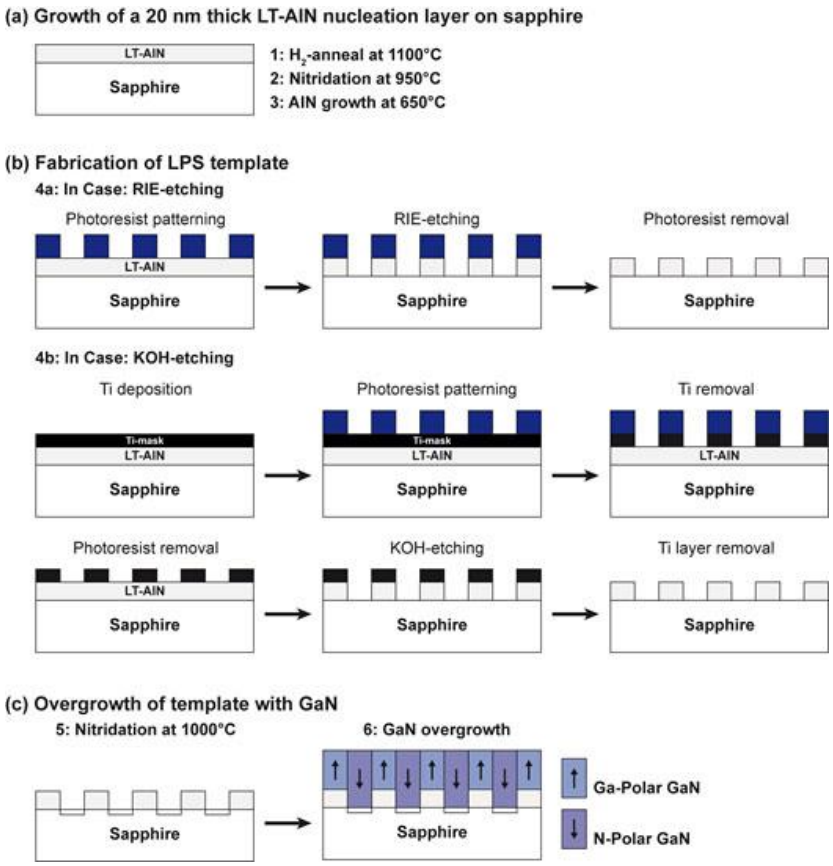

Fig. 1: 3-step Fabrication process of a GaN based lateral polar structure. (a) Growth of a 20 nm AlN buffer layer. (b) Fabrication of the template including photoresist patterning and etching with KOH and RIE. (c) GaN overgrowth of the patterned template with MOCVD results in lateral polar structures.

The second step includes the patterning of the AlN nucleation layer into periodic stripes or circles by lithography and etching techniques as displayed in Fig 1 (b). Two different etching techniques were used: wet etching in potassium hydroxide (KOH) or reactive ion etching (RIE). The pros and cons of the two etching methods will be presented later. The lateral p/n-junctions of Chapter 4 were mostly fabricated using RIE etching. The patterning used a lithography mask consisting of stripe widths of 5000 µm, 50 µm, 20 µm, and 5 µm that were oriented in two directions: parallel and perpendicular to the a-plane of sapphire. The two different etching methods required slightly different patterning. In case of the KOH etching, a thin Ti-layer (~30 nm) was required as a mask and was deposited by e-beam evaporation. The

Ti-layer was patterned using standard optical lithography and 5% HF. Subsequently, the remaining Ti-mask was removed using 5% HF. This procedure on the LT-AlN layer resulted in a template with periodic LT-AlN and bare sapphire stripes side-by-side. Alternatively, in the case of RIE etching, the fabrication involved a similar patterning process but without the use of the Ti-layer; here, photoresist served as a mask. After patterning, the RIE etching was done. The removal of the photoresist after etching resulted in a periodic structure similar to the one produced with KOH etching. After etching, all patterned samples were rinsed in deionized water and blown dry with nitrogen before reintroduction into the MOCVD chamber.

The influence of the etching of the AlN in the second fabrication step on the quality of LPS templates has been investigated. The RIE shows better etching results for small domain sizes in the micrometer range. RIE results in sharp edges of the LT-AlN domains. In contrast, KOH etching during the fabrication process leads to side etching of the LT-AlN stripes. This results are shown in Fig. 2 (a) and (b).

Fig. 2: AFM images of KOH (a) and RIE (b) patterned templates for lateral polar structures (the same AFM scale applies for both pictures).

In the third fabrication step of an LPS, the templates were overgrown with AlGaN using the MOCVD reactor. The GaN growth conditions were critical for simultaneous growth of both polarities of GaN as it will be discussed later below. The GaN films were 1.3 µm thick. For the growth of AlGaN LPS with high Al content, there is a changed growth process in comparison to GaN and AlN LPS growth. AlGaN LPS growth needs the deposition of a HT-AlN nucleation layer to avoid cracking prior to the overgrowth. The overgrowth for AlGaN LPS can be seen in Fig. 3. The 50 nm thick high temperature (HT)-AlN film was grown at 1250°C, resulting in III-polar domains with underlying LT-AlN and N-polar domains with underlying sapphire. On top of the HT-AlN, a 600 nm $Al_xGa_{1-x}N$ layer was deposited. The Al composition of the $Al_xGa_{1-x}N$ Layer was varied between 0.6 - 1.0.

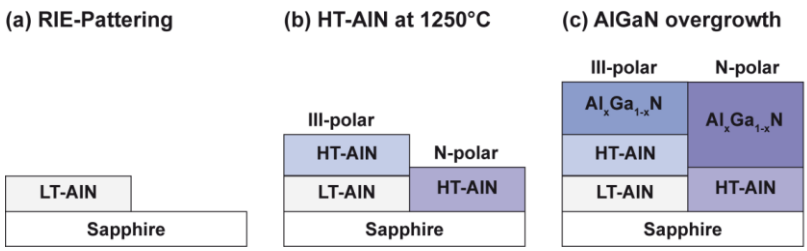

FIG. 3: Growth process of AlGaN based Lateral Polar Structures. (a) RIE patterning. (b) Growth of HT-AlN. (c) Overgrowth of HT-AlN with AlGaN.

This work was published in: M. P. Hoffmann, M. Gerhold, R. Kirste, A. Rice, C.-R. Akouala, J. Q. Xie, S.

Mita, R. Collazo and Z. Sitar, Proceedings of SPIE **8631**, 86311T (2013).

3. Growth and characterization of GaN LPS

The LPS consists of Ga- and N-polar GaN grown with MOCVD side-by-side separated by an inversion domain boundary (IDB). It has been demonstrated that under typical growth conditions, GaN growth is mass transport limited, thus the growth rate should be independent of the polar orientation. However, some observations suggest that a difference in the growth rate between the domains exists under certain conditions, especially when the two polar orientations are grown in close proximity. This has led to contradictory conclusions in literature suggesting that there is an intrinsic growth rate difference between the two polar orientations.

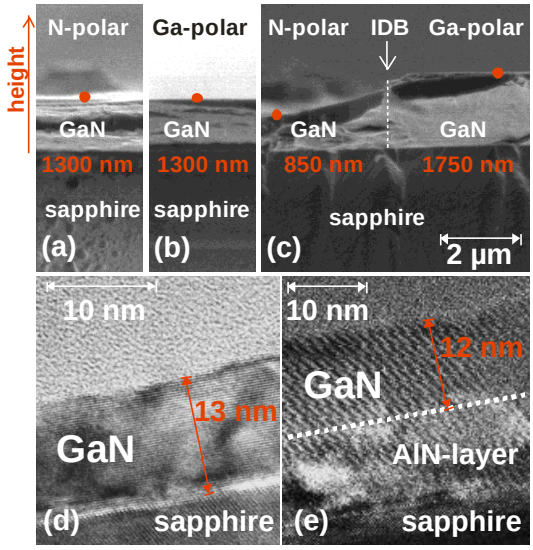

Figure 4: Cross-sectional SEM images of a GaN film with N-polarity (a) and Ga-polarity (b) grown on a sapphire substrate and of a GaN film grown on a patterned LT-AlN/ sapphire substrate in the area of the inversion domain boundary (c). TEM of an N-polar (d) and Ga-polar (e) film with growth interrupted after 30 s (note the different scales in (d) and (e)).

Fig. 4 (a) and (b) show cross-sectional SEM images of either a Ga- or N-polar GaN films grown on a unpatterned substrate. The Ga-polar film is typical with a smooth surface morphology, while for the N-polar film the surface morphology is characterized by hexagonal hillock structures. For both films, the overall thickness can be estimated to be approximately 1300 nm, with a small variation of less than 100 nm over the complete substrate area. In this respect, no difference in the growth rate is observed between the N- and Ga-polar GaN films. This finding is supported by TEM in Fig. 4, where a N- (d) and Ga-polar (e) GaN film is shown after deposition of only 30 s. Both films are fully coalesced with a comparable thickness of 12 to 13 nm, indicating identical growth and nucleation rates. Fig. 4 (c) shows a cross-sectional image of a GaN film grown on a patterned LT-AlN/sapphire wafer. It should be mentioned that this film was grown using the same growth time and process conditions as the films grown on the unpatterned substrates (a) and (b). Fig. 4 (c) corresponds to the area of the inversion domain boundary of a LPS with stripes of 10 µm width. Despite the same growth time, the thicknesses of the N- and Ga-polar domains of the LPS are 850 nm and 1750 nm, respectively. This shows that each domain has a different thickness than the corresponding films grown on unpatterned substrates with thickness of 1.3 µm. This is

in addition to the observation that the thickness is also different between the two different domains. Due to this height difference a step can be observed at the IDB. It is important to note that if the overall mass of both a 10 µm wide N- and Ga-polar stripe were added up, it would correspond to the total mass that would be expected for a 20 µm wide region from the GaN films grown on the unpatterned substrates. In other words, the overall mass within the LPS stripe is conserved despite the different thicknesses of each domain. As the growth conditions are within the mass-transport limited regime, with sufficient incorporation sites and atomic diffusion lengths, the total deposited mass is expected to be constant independent of polar orientation. Thus, the observation of a thickness difference between N- and Ga-polar GaN in a LPS is not due to either an intrinsic difference in the growth rate or a nucleation rate difference between the two polarities. Therefore, in order to explain the observed height difference, a macroscopic mass transport between the N-polar to the Ga-polar domains during growth is required to occur.

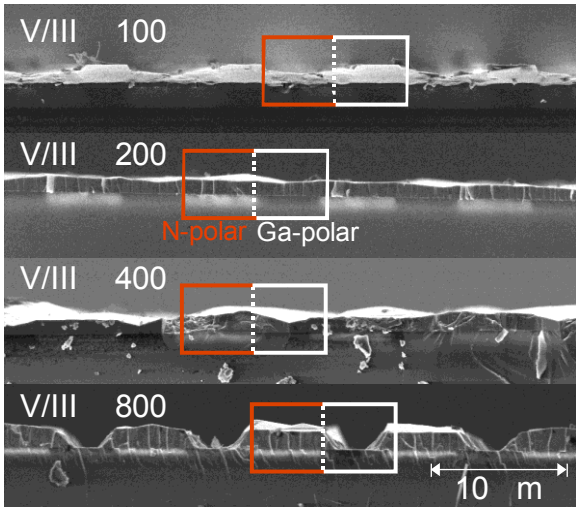

Fig. 5: SEM cross-sectional images of LPS samples grown under different V/III ratios in the region of the IDB. The red box marks the position of one of the N-polar domains and the white box marks that of one of the Ga-polar domainss. The dashed line indicates the position of an IDB. Periodicity of the LPS is 5 µm.

In order to understand the mass transport between N- and Ga-polar GaN, LPS were prepared under different V/III ratios while the rest of the reactor parameters remained unchanged. Fig. 5 shows SEM cross-section of LPS samples grown under V/III ratios of 100, 200, 400 and 800. All images correspond to domains with stripe width of 5 µm (periodicity 10 µm). A typical N-polar domain is marked red and a Ga-polar domain is marked white; a vertical white dashed line denotes the IDB between the domains. Similar to the results presented in Figure 4, the LPS sample grown under a V/III ratio of 100 reveals an average thickness of 0.8 µm and 1.7 µm for the N-polar domain and the Ga-polar domain. If the V/III ratio is increased to 200 the height difference reduces and both polarities have a comparable thickness of around 1.3 µm which is close to the value measured for the layers grown on the full wafers (Fig. 4 (a) and (b)). A further increase of the V/III ratio to 400 leads to an increase of the thickness of the N-polar film at the expense of the Ga-polar domain. Finally, at a V/III ratio of 800, only N-polar GaN is grown with a thickness of ~1.4 µm, while the deposition at the Ga-polar domain may have been insignificant. Furthermore, using different stripe orientations and KOH etching, it was demonstrated that this material corresponds to lateral growth of the N-polar GaN domain on the a-facet of the N-polar stripes. Thus no Ga-polar GaN is grown within the 5 µm wide stripe region at the V/III ratio of 800.

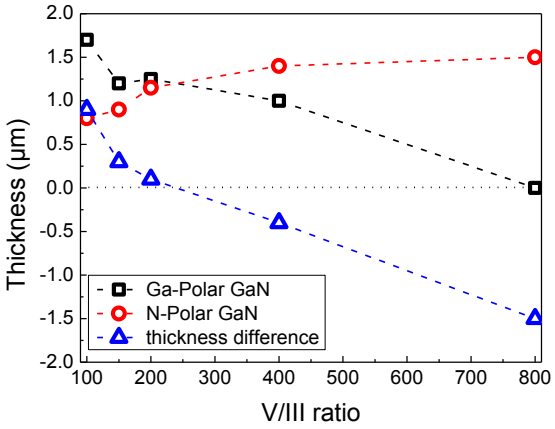

Fig. 6: Thickness of the Ga-polar and N-polar domains of LPS close to the IDB and resulting thickness difference depending on the applied V/III ratio during growth.

Fig. 5 summarizes the observations from cross-sectional SEM imaging by displaying the thickness of the N- and Ga-polar domains in the LPS as well as the thickness difference as a function of the V/III ratio used during growth. These values correspond to the average height of the stripes. Therefore, the variation of the V/III ratio leads to different layer thicknesses of N- and Ga-polar domains, if grown as an LPS. Except for the LPS grown under a V/III ratio of 800, the film thickness of the GaN layers, if averaged over the N- and Ga-polar domain, is 1.1 to 1.3 µm. This value corresponds to the measured film thickness of the films grown on unpatterned substrates. Again, this further supports the observation that the height difference near the IDB the overall mass of the GaN is conserved for the used growth conditions. Furthermore, based on the data in Fig. 6, it is suggested that same height LPS can be achieved at V/III ratios around 230.

It was observed that despite the commonly observed height difference in LPS, the overall mass of the N- and Ga-polar domain was constant and that the height difference can be controlled by changing the growth conditions. These observations imply that there is no difference in the intrinsic growth rate between Ga- and N-polar GaN, as it is proposed by some works. It was pointed out that the mass conservation during the LPS growth is related to mass transport limited conditions and that the height difference must be related to some mass transport between the domains of opposite polarization.

In general, mass transport across a crystal surface during MOCVD growth is determined by a balance of the flux from the vapor phase to the surface, the flux from the surface back to the vapor due to desorption, and the flux along the surface. For the MOCVD growth of GaN, only the flux of the Ga-species needs to be considered, as the V specie is typically available in excess. Taking into account the growth under mass transport limited conditions, the net flux towards the surface (difference between the flux from vapor to the surface and desorption flux) is equal to the diffusion flux along the surface towards atomic incorporation sites (i.e. step edges).

The net flux towards the surface is dependent on the vapor supersaturation which is directly controlled by the growth conditions (i.e. V/III ratio). Thus, since the net flux towards the surface and the diffusion flux along the surface are equal, the latter can be influenced by the growth conditions. The diffusion along the surface is a combination of atomic surface diffusion and macroscopic mass transport (surface diffusion flux). The first is dependent on the surface, which includes among others the actual growth mode, roughness, and polarity. However, for a given temperature, the atomic surface diffusion does not depend

on the growth conditions such as V/III ratio. Furthermore, the corresponding length scales are expected to be rather short (as much as 100 nm) with respect to the stripe sizes. Thus, the two different polar surfaces are expected to have different corresponding atomic surface diffusion lengths, but the atomic surface diffusion is not expected to play a major role in the formation of the height difference in LPS.

The macroscopic mass transport, which also contributes to the diffusion flux along the surface, directly depends on the surface adatom concentration gradient and is dependent on the growth conditions, even at a constant temperature. Thus, a mass transport critical length due to the actual macroscopic mass distribution profile can be defined, as function of growth conditions. This critical length is associated to the macroscopic mass diffusion length. Typical lengths scales for the macroscopic mass diffusion length and the mass transport critical length are expected to range from few micrometers up to a few millimeters. However, temperature and other growth parameters can be used to control and manipulate this critical length.

Following these considerations, a model is proposed in which N- and Ga-polar GaN surface have a different critical length (related to the mass diffusion length) which can be manipulated by the applied growth condition such as V/III ratio. In this model, Ga atoms will diffuse for micrometers along the N- and Ga-polar surface and across the inversion domain boundary before they are adsorbed. The domains with the longest associated critical length will have a negative net mass flux, that is, material will be lost from the domain towards the other domain.

However, it could be shown that the mass transport between the domains can be controlled and GaN LPS with domains of equal height could be fabricated. These results will be published in:

J. Rajan, R. Kirste, M. Hoffmann, W. Guo, I. Bryan, L. Hussey, M. Gerhold, S. Mohn, M. Albrecht, R. Collazo and Z. Sitar, “Controlled mass transport between Ga- and N-polar domains in GaN lateral polarity structures”, Journal of Applied Physics, manuscript in preparation.

4. Growth and characterization of AlGaN LPS

$Al_xGa_{1-x}N$ LPS with high Al content are highly desired because of their low absorption in the deep UV in comparison to GaN LPS. Therefore, $Al_xGa_{1-x}N$ LPSs with varying Al composition have been grown aside GaN LPS. Well defined domains and boundaries with stripes of 50 µm, 20 µm, 10 µm and 5 µm could be observed for all compositions. A SEM image of an $Al_{0.7}Ga_{0.3}N$ LPS with 5 µm stripes is shown in Fig. 7. The two types of domains show no overgrowth or lateral growth; darker regions are III-polar $Al_{0.7}Ga_{0.3}N$ while brighter regions are N-polar $Al_{0.7}Ga_{0.3}N$. This observation suggests a successful patterning of the LT-AlN nucleation layer and a successful polarity control of III- and N-polar domains, while overgrowing the LT-AlN and c-sapphire domains with AlGaN.

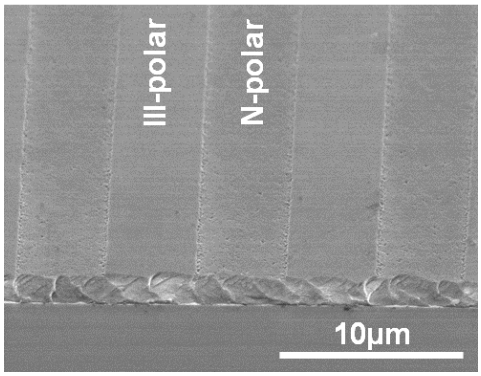

Fig. 7: SEM image (60° tilt) of an $Al_{0.7}Ga_{0.3}N$ LPS with domains of 5 µm.

To verify the polarity of the $Al_xGa_{1-x}N$ LPS domains, KOH etching has been used. N-polar AlGaN is etched by KOH, while III-polar AlGaN shows no detectable etching. In Fig. 8, an $Al_{0.8}Ga_{0.2}N$ LPS has been displayed, (a) before and (b) after KOH-etching. KOH removes in (b) the N-polar AlGaN domains completely, while the III-polar domains have not been etched. Fig. 7 also confirms that the inversion domain boundary (IDB) between the polar domains is well defined through the applied LPS fabrication method, suggesting applicability of the LPS for QPM

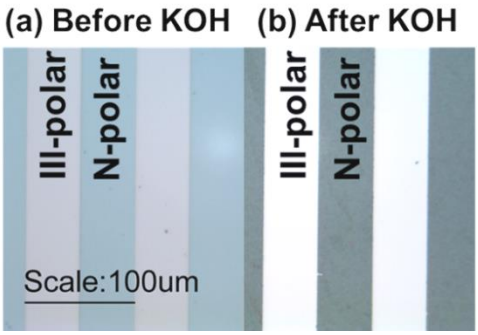

Fig. 8: Microscope image of an $Al_{0.78}Ga_{0.22}N$ LPS with domains of 50 µm (a) before and (b) after KOH etching.

For further investigation on the $Al_xGa_{1-x}N$ LPS, the impact of Al composition on the structural quality has been investigated by SEM, AFM and XRD. XRD measurements have been used to determine the Al compositions. SEM imaging at the inversion domain boundary reveal a significant difference in surface morphology and a height difference between the polar domains depending on the Al content in the LPS. In Fig. 9 the SEM images of $Al_xGa_{1-x}N$ LPS with varying Al composition is presented. The III-polar domains of all $Al_xGa_{1-x}N$ LPS show a smooth surface. However, the Al composition in the AlGaN LPS significantly impacts the surface morphology in the N-polar domain. N-polar domains have rough surfaces. Lower Al compositions lead to a smoother surface in the SEM images. An increase of Al composition in the LPS leads, in contrast, to an apparent columnar structure in the N-polar domains, especially in the AlN LPS. Nevertheless, it will be shown in the next chapter that the N-polar films in the AlN LPS consists of fully coalesced N-polar material, even though it apparently has columns at the growth surface. This observation will be explained as difference in growth mode between the two

domains. A two dimensional growth mode can be found in the III-polar and a 3D columnar growth mode can be observed in N-polar domains. As the Al composition increases in the N-polar $Al_xGa_{1-x}N$ domains, a more 3D columnar-like growth can be observed. The N-polar surface of the $Al_{0.6}Ga_{0.4}N$ in contrast to AlN is fully coalesced and shows no columnar structure.

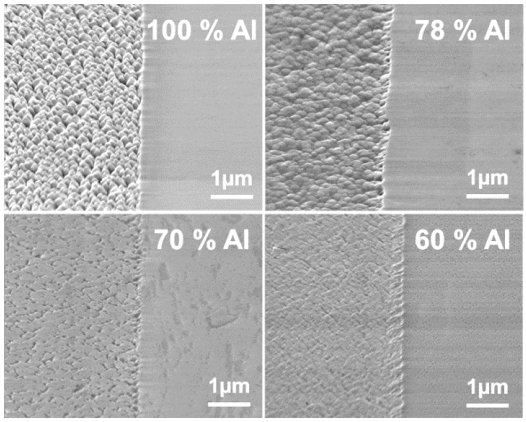

Fig. 9: SEM images at the IDB of $Al_xGa_{1-x}N$ LPSs with varying Al compositions (0.6 to 1.0). The domain size of the LPSs are 5 µm. Left domains are N-polar; right domains are III-polar.

The surface morphology was also investigated by AFM. In Fig. 10, a line-scan from a III- to a N-polar domain is shown, as well as a two dimensional AFM image (20 x 20 µm) of the surface of the $Al_{0.78}Ga_{0.22}N$ LPS. The III-polar surface is found to have a RMS value of 0.3 nm (5 x 5 µm scan) for all $Al_xGa_{1-x}N$ LPS. The RMS value for the N-polar domain of the $Al_{0.78}Ga_{0.22}N$ LPS can be found to be about 8 nm. The RMS value increases for the N-polar domains from 4 nm to 15 nm as function of Al composition (0.6 to 1.0) in agreement with SEM observations. In addition, the AFM line scans can be used to reveal the height differences between the polar domains (e.g. $Al_{0.78}Ga_{0.22}N$ around ~85 nm).

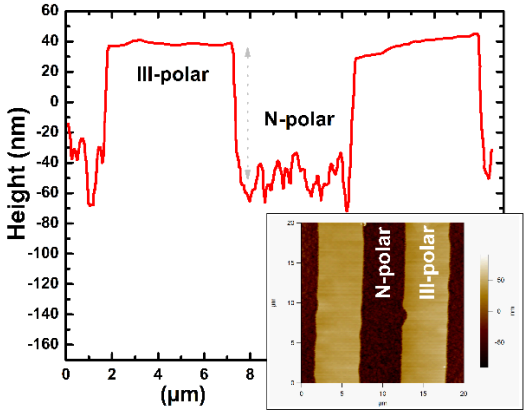

Fig. 10: AFM line-scan at the IDB from III-polar to N-polar AlGaN domains (5µm stripes). The inset picture shows the two dimensional AFM image of the surface of the $Al_{0.78}Ga_{0.22}N$ LPS.

Fig. 9 and Fig. 10 showed that the height difference observed between the N- and III-polar domains depended on the composition. A lower Al content in the LPS leads to a larger height difference. The

height difference as function of Al composition is presented in Fig. 11. The height difference value has been determined by AFM line scans at the IDB for all LPSs. While low Al content $Al_xGa_{1-x}N$ LPS show a significant height difference, an AlN LPS shows no height difference at all (will be discussed in detail in the following chapter). The small difference observed in Fig. 11 corresponds to the underlying LT-AlN nucleation layer for the III-polar domains. This observation highlights that for an AlN LPS no significant growth rate difference can be found, in contrast to findings when growing GaN LPS. A linear fit of the graph in Fig. 11 leads to a suggested height difference for GaN of ~270 nm in agreement with reported growth rate differences for GaN LPS grown under similar conditions.

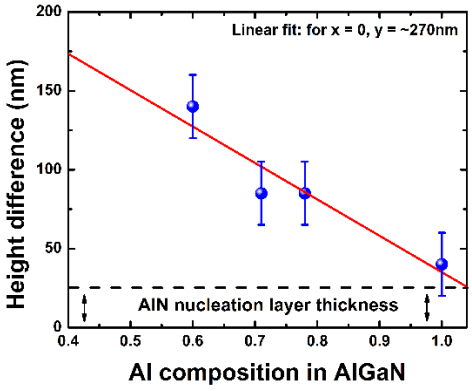

5.

Fig. 11: Height difference between N-polar and III-polar domains as function of the Al composition in an $Al_xGa_{1-x}N$ LPS.

The growth rate difference between the polar domains observed for $Al_xGa_{1-x}N$ LPS is strongly dependent on the Ga content in the alloy. This follows from the realization that the composition change, from high to low Al content, was simply achieved by increasing the TEG flow. Other growth conditions like TMA flow, V/III-ratio, temperature, pressure, etc. were kept constant. Increasing the Ga content led to a decrease in the growth rate of the N-polar domain leading to a height difference. In GaN based LPS, a strong dependence of the growth rate and therefore a height difference of the domains, can be observed as a function of the applied V/III-ratio. On the other hand, there is no height difference for AlN based LPS. This strongly suggests that the height difference is critically dependent on the applied Ga-supersaturation and the corresponding response to the Ga incorporation on both domains. Thus, for AlGaN LPS with high Ga content, a higher Ga incorporation on the III-polar domains due to the response to the Ga-supersaturation could be responsible for the observed height difference. It has been observed that there is a large height difference between domains in GaN at relatively low V/III-ratios in the last chapter. $Al_xGa_{1-x}N$ LPS have been grown with relatively low V/III-ratios (below 200); similar to growth conditions where GaN LPS show a higher growth rate for Ga-polar domains relative to the N-polar domains.

Nevertheless, the presented $Al_xGa_{1-x}N$ LPSs have indeed shown a promising high quality to be used for SHG in the UV. The well-defined periodicity of LPS stripes in the micron-range and the quality of the boundary between the polar domains lead to low scattering losses when the AlGaN LPS are used for quasi phase matching. The height difference between the domains could be controlled by the growth conditions (V/III-ratio) as shown for GaN LPS.

The presented results of this chapter will be published in:

M. P. Hoffmann, R. Kirste, S. Mita, W. Guo, J. Tweedie, I. Bryan, Z. Bryan, M. Gerhold, R. Collazo, and Z. Sitar, "Growth and characterization of $Al_xGa_{1-x}N$ lateral polarity structures", manuscript sent to Physica Status Solidi (b).

6. Growth and characterization of AlN LPS

AlN is a useful material system for optical and electronic applications because of the wide bandgap and its UV applications. Devices have been demonstrated based on Al-polar AlN, since this polar orientation indicates low defect incorporation and increased doping possibility in comparison with N-polarity. In addition especially for electronic applications and sensors, the use of N-polar AlN might be also desirable because of low Schottky barrier heights and a low contact resistance. Nevertheless, control of both polarities and growth of AlN polar domains in proximity, like in a lateral polarity structure (LPS), have not been demonstrated. AlN-based LPS are, as mentioned above, useful for UV-laser light conversion via SHG, but in addition a new class of devices like high-power and high-frequency hetero field effect transistors and high-power UV-LEDs could be also fabricated by the use of AlN LPS. The advantage of the use of AlN in comparison to pure GaN for LPSs lies in the transparency of AlN in the deep UV range (~ 200 nm). AlN LPS are beneficial for frequency doubling in the deep UV were GaN cannot be used. It has to be noted that AlN LPS for SHG also allow for wider periodic gratings in comparison to GaN, because of a lower refractive index difference in the UV. In this section a summary of the fabrication procedure of AlN LPSs along with characterized of their properties will be described.

A 600 nm AlN thin film was grown by metalorganic chemical vapor deposition on sapphire. In order to control the polarity, a LT-buffer layer was grown at 650 °C. The buffer layer was patterned by RIE etching leading to a partial removal of the LT-AlN. Subsequent growth of high temperature (1250 °C) AlN resulted in Al-polar domains in areas with an underlying LT-AlN layer and N-polar AlN where the buffer layer was removed, similar to the polarity control schemes already demonstrated for GaN. Samples were grown at 80 Torr in a hydrogen atmosphere with a NH_3 and trimethylaluminium (TMA) mass flow of 4.46 mmol/min and 21 µmol/min, respectively. Domain sizes ranging from 5 µm up to 5 mm were achieved for both domain types, as determined by the mask feature sizes.

Fig, 12 (a) shows a cross sectional SEM image of an AlN LPS around the inversion domain boundary (IDB) is presented. The III-polar domain is fully coalesced and exhibits a smooth surface with few defects. This observation is consistent with results in GaN LPS. In contrast to the III-polar films, the N-polar film in (a) left consists of multiple columnar like structures that are not coalesced near the surface. Here a two-dimensional growth mode is expected for the Al-polar film while the N-polar AlN would tend to grow in a columnar morphology leading to the observed rough surface. Nevertheless, the IDB between the Al- and N-polar domains is well defined as shown in Fig. 12 (b). Even for the small stripe size of 5 µm, sharp interfaces and well-defined domains can be produced. This is most important for SHG and conversion into the deep UV, when LPS are uses for frequency doubling.

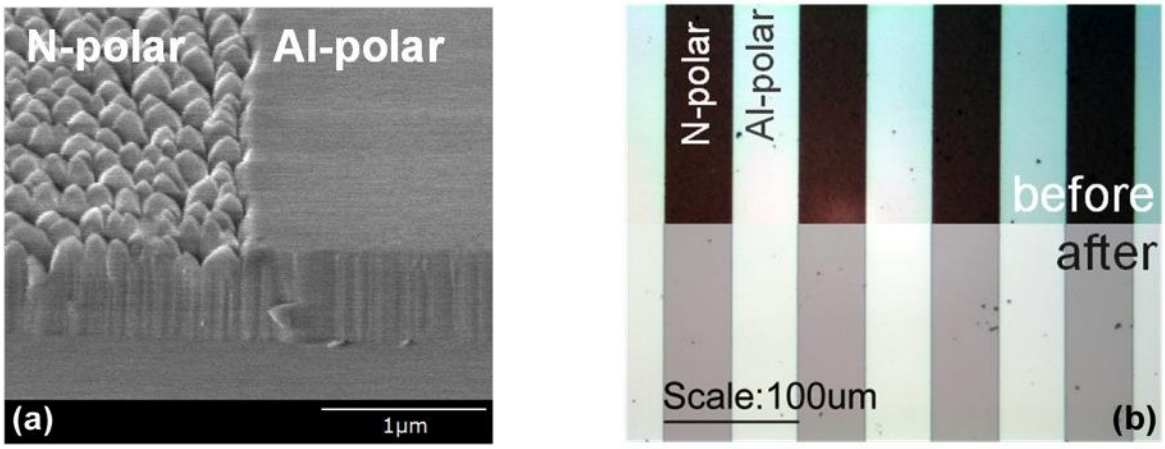

Fig. 12: Characterization of a 600 nm thick AlN LPS at the IDB. (a) SEM image (60º tilted) with domains of N- and III-polarity. (b) Microscope images of AlN LPS before (top) and after (bottom) KOH etching for determination of polarity.

Fig. 12(b) shows the results of KOH etching at 70ºC for determination of polarity. The etching was performed on 50 µm wide stripes. The top of the image in (b) represents the AlN LPS before the etching and the bottom of the pictures is an AlN LPS that has been wet etched with KOH. No etching can be examined on the Al-polar domains, but the N-polar domains are fully removed by the KOH.

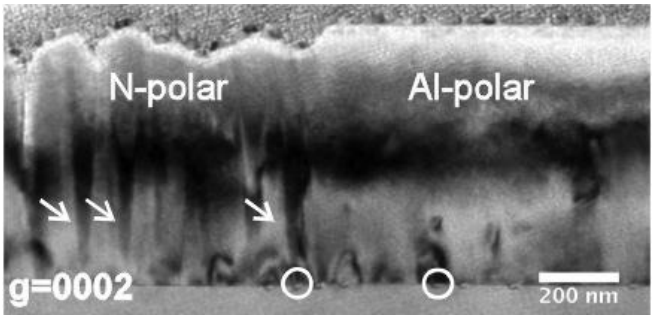

Fig. 13: Bright field TEM image of an AlN LPS at the IDB with the N-polar region on the left and the Al-polar region on the right.

In order to investigate the columnar structures and the quality of the AlN films, a bright field transmission electron microscopy (TEM) measurement was performed on the AlN LPS close to the IDB. Fig. 13 shows the TEM image of a lateral boundary with a g-vector parallel to the c-axis of the same sample that has been characterized previously by SEM. The above observed columns for the N-polar domain can be observed and it can be determined that the N-polar film is coalesced within the first 300 nm–400 nm. The white circles in Figure 4 indicate voids in the sapphire substrate. This will be described in the next section. In addition, the dislocation density was determined for the Al-polar and N-polar domains. In both domains a low density of screw-type dislocations could be found and most dislocations are of mixed type. Similar densities of dislocations are found for both polarities of $1x10^{10}$ cm^2 representing a typical value for Al- and N-polar AlN grown on sapphire that can be found in the literature**.** In the case of N-polar films, most of the dislocations bend near the sapphire interface leading to a strongly reduced dislocation density at the film surface. In contrast in the Al-polar film, the dislocation bending is not as pronounced.

To compare and investigate the point defects in the Al- and N-polar domains, low temperature (5 K) photoluminescence spectra were recorded. The deep defect luminescence is presented in Fig. 14 (a). An intense luminescence can be found for the N-polar film at 3.5 eV, 3.2 eV, and 4.4–4.7 eV which were assigned to silicon, oxygen and Al-vacancies, respectively. This luminescence is an order of magnitude more intense in comparison to the Al-polar AlN film. This suggests that similar to N-polar GaN or InN, an increased point defect incorporation occurs on the anion side in N-polar AlN. Figure 14 (b) shows the representative spectra of the near band edge luminescence for the two polarity types. Surprisingly, the free exciton emission is dominating the spectrum even at low temperatures. This is not expected since all excitons are expected to be bound to impurities. Similar observations were made previously for AlN grown on sapphire. In contrast, homoepitaxial grown AlN layers on AlN do not indicate this observation and the bound exciton transitions dominate the spectra. More detailed investigations will be needed in the future to explain this unexpected observation. However, for the Al-polar domains the same emission lines can be observed in (b) as for the N-polar domains. Nevertheless, the peak positions are considerably shifted to higher energies and broadened for the Al-polar film (e.g. X_A from 14.3 meV to 22.3 meV). This suggests a higher optical quality of the N-polar in comparison to the Al-polar domains, since broadening is typically explained by the decreased crystal quality of films.

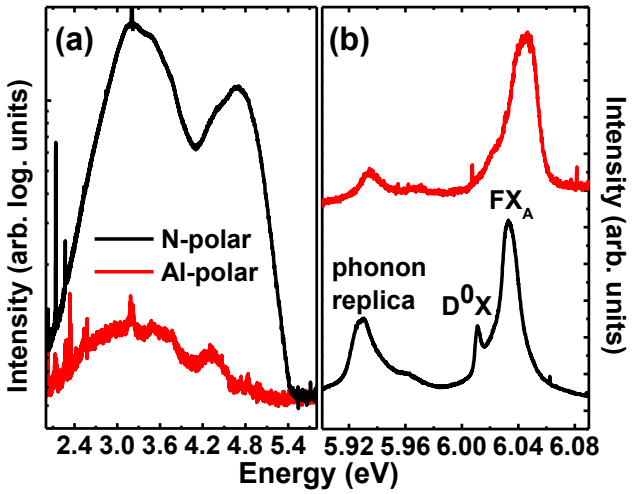

Fig. 14: Photoluminescence at 3K of an AlN LPS. (a) The deep defect luminescence region. (b) The near bandgap free and bound exciton transitions. Note that the y-axis in (a) is in logarithmic scale.

In conclusion, it was demonstrated in this section that AlN LPS could be grown following the typical polarity control scheme as implemented for the growth of GaN LPS. SEM and TEM images revealed a columnar appearance of the N-polar domain that is coalesced near the sapphire interface. A 3D-like growth mode for the N-polar films lead to a lowering of the dislocation density, decreased strain and better optical quality in comparison to the Al-polar films. The results for the AlN LPS will allow for a new class of AlN-based lateral polarity devices similar to those proposed for GaN. A smoother surface for the N-polar domains are desired since the roughness of the N-polar domains leads to scattering effects when the LPS is used for SHG and light is propagated laterally through the structure. Future work will focus on low temperature growth to reduce the void formation and, therefore, decrease the formation of inversion domains. In addition, the effect of temperature on the columnar growth for the N-polar domains should be investigated.

This work was published in: R. Kirste S. Mita, L. Hussey, M. P. Hoffmann, W. Guo, I. Bryan, Z. Bryan, J. Tweedie, J. Xie, M. Gerhold, R. Collazo and Z. Sitar, "Polarity control and growth of lateral polarity structures in AlN", Applied Physics Letters **102**, 181913 (2013).

7. Optical characterization of AlGaN waveguides

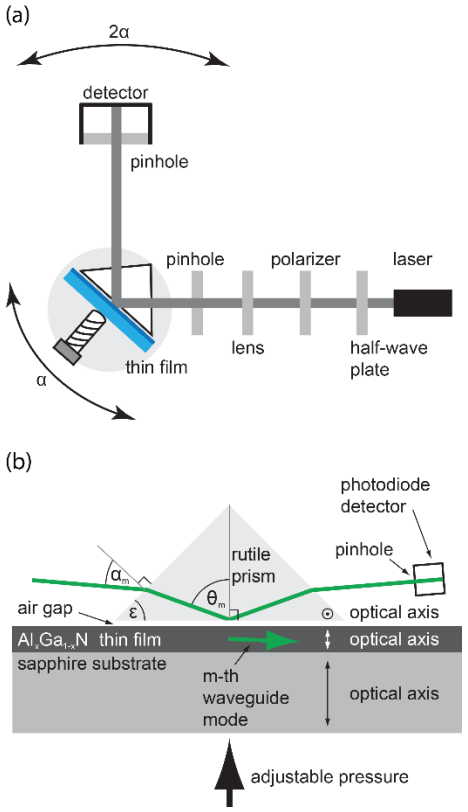

Fig. 15. Schematic of the prism-coupling set-up. (a) Polarization of the laser is adjusted and the beam is focused onto a prism base to a spot size of 50 µm. The reflected signal is measured by a photodiode; a pinhole is used to block the beams originating from internal reflections in the prism. (b) Enlarged view of the prism coupling setup to launch a single guided mode *m* into the AlGaN waveguide. The film, the sapphire substrate and the rutile prism are optically uniaxial with the direction of the axes as marked in the figure. A symmetric rutile prism with an apex angle ε of 45.00° is used.

The refractive index and its dispersion determine the QPM structure periodicity for a particular wavelength. In order to design and grow these structures and calculate achievable conversion efficiencies, an exact knowledge of the refractive index for both polarities of AlGaN over a wide compositional range is needed. In addition, a possible difference in the refractive indices between III-metal-polar and N-polar AlGaN would cause reflection losses at every interface between the domains of opposite polarity, which would drastically reduce the conversion efficiency of the SHG structure. As the two different polar surfaces incorporate point defects at a different rate during growth, the refractive index at the wavelengths of interest may be different for the two polar domains. This part of the work determined the ordinary and extraordinary refractive indices of III-polar and N-polar $Al_xGa_{1-x}N$ ($0 < x < 0.30$) using the prism coupling technique. It was found that Sellmeier equations could be used to fit the energy dependence of the refractive index over a very broad wavelength range.

The prism coupling method was used to determine the refractive indices of the thin film waveguides. A schematic drawing of the setup is displayed in Fig. 15. In this method, light is coupled into the waveguide under different angles of incidence and the intensity of the reflected light is measured. A strong coupling of the incident beam into the film occurs when the component of the impinging wave vector parallel to

the layer surface meets the propagation constant of a distinct waveguide mode (m = 0, 1, 2…), leading to a decrease of the intensity of the reflected light. The minima-positions in the reflected intensity depend on the waveguiding properties of the layer, allowing for simultaneous determination of the refractive index and thickness. In addition, by using both polarizations of the incoming light (TE: electric field polarized parallel to the film surface, TM: electric field polarized approximately normal to the film surface), birefringence of the film can be obtained if the film is thick enough to support at least two guided TE and TM modes. An example of a typical measurement is shown in Fig. 16. The prism angles α_m are then transformed to coupling angles θ_m by taking into account the refraction on the prism surfaces. It should be mentioned that even though the coupling condition is optimized for a specific m-mode, also all the other modes are weakly excited due to optical scattering inside the film.

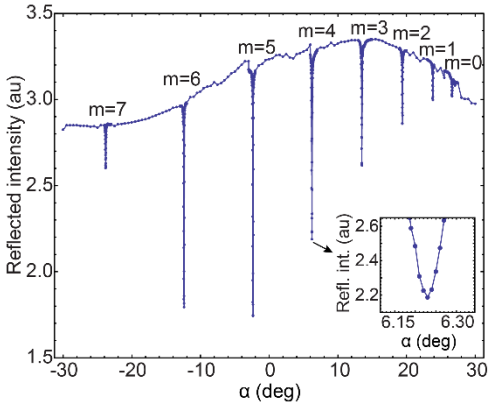

Fig. 16: Coupling curve for the III-metal-polar GaN sample at 532 nm for TE polarization. The sharp dips at the coupling angles indicate very high optical crystal quality. The angular resolution of the measurement around the coupling angles was 0.01 degrees.

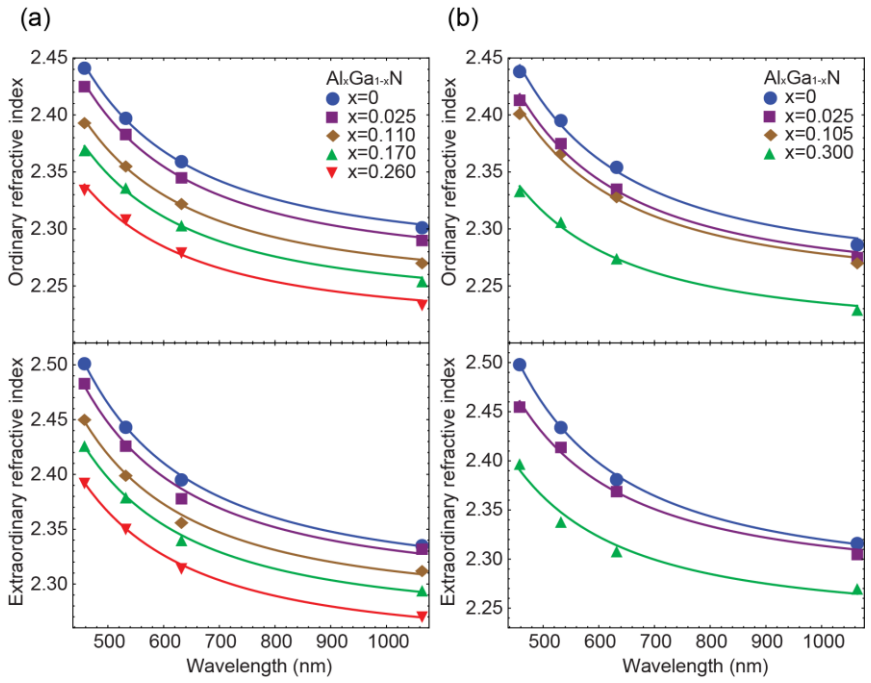

Fig. 17: Wavelength dependence of ordinary and extraordinary refractive indices for AlGaN with different Al-concentration. (a) III-metal-polar samples, (b) N-polar samples. Symbols represent prism coupling measurements at discrete wavelengths and the curves are first-order Sellmeier fits.

Fig. 17 shows the measured refractive indices using the prism method along with a fit to the first-order Sellmeier formula. The dispersion of ordinary and extraordinary refractive indices was measured at four wavelengths between 458 and 1064 nm in samples with the Al concentration up to 0.30. The dispersion was described well by the first-order Sellmeier equation. In addition, a small difference in refractive indices between the two materials with different polarity was observed, which probably arose due to different impurity levels in films of different polarity.

This work was published in: Rigler et al., "Refractive index of III-metal-polar and N-polar AlGaN waveguides grown by metal organic chemical vapor deposition", Appl. Phys. Lett. 102, 221106 (2013).

8. SHG measurements

The experimental system for second harmonic generation in AlGaN waveguides consists of femtosecond pulses with tunable central wavelength that are coupled into a fabricated waveguide by end-fire coupling technique. The SHG signal generated in the waveguide is out-coupled and analyzed with a spectrograph and a photon counting camera. Femtosecond pulses from Opera Solo are directed to the end-fire coupling system designed for the SHG experiment (Fig. 18). The intensity of the laser beam is attenuated with the suitable neutral density filter. With the beam expander the beam diameter is adapted to the size of the in-coupling lens for efficient focusing. A spherical diffraction-limited coupling lenses have the numerical aperture of 0.55, working distance of 1.7 mm and a clear aperture of 8mm. The coupling lenses and the custom made sample holder were mounted on a *xyz*-translators, which enabled precise positioning of the focal point of the laser beam. The efficiency of the coupling was constantly monitored with two CCD cameras. One was fitted with a microscope objective and was mounted above sample on the 3-axis translator stage. The second camera without an objective was used after the out-coupling lens, allowing the analysis of the beam shape of out-coupled light. A proper spectral filtering (short pass filter) is necessary in order to remove strong fundamental light, allowing us to examine the SHG wave generated in the waveguide. The SHG signal is then directed to the detection system.

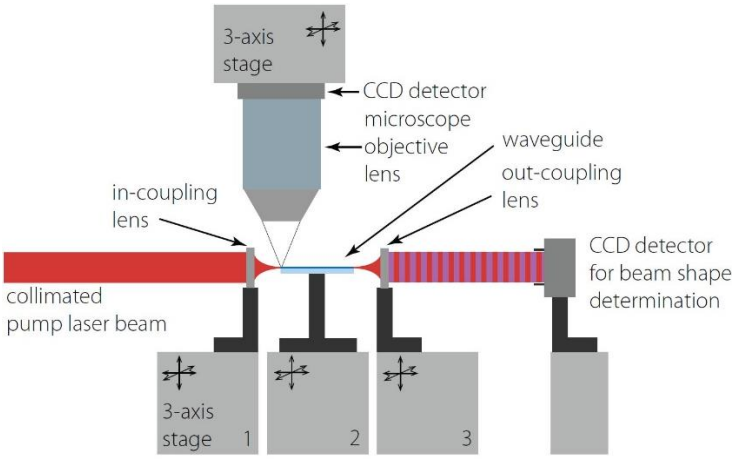

Fig. 18: Edge coupling system for second harmonic generation in AlGaN waveguides. Coupling lenses and custom made sample holder are mounted on a xyz translators, which enables precise positioning of the focal point of the laser beam onto the front facet of the waveguide. The efficiency of the coupling is constantly monitored with two CCD detectors.

As a detector of the obtained SHG signal a spectrograph and a CCD photon counting camera was used. The Spectral analysis was done with SpectraPro-2300i spectrograph with the following properties. Two different gratings are installed in the device and used depending on the type of the experiment: a 600

grooves per mm with the blaze wavelength of 1 μm and a 1200 grooves per mm with the blaze wavelength of 500 nm. Andor iStar CCD camera was used for detection of the signal coming out of the spectrograph. It has a CCD head with 2048 × 512 pixels and square pixel size of 13.5 μm2. The CCD detector was cooled down to −30 °C in order to reduce dark current. Camera was operating in the gated regime which was synchronized with the Legend repetition rate. The time delay between the SHG signal and the trigger pulse from the Legend was 18 ns which was the optimum with respect to all beam paths and cable lengths. The width of the detection gate was set to 5 ns. The in and out coupling of the light into the waveguide is presented in Fig. 19. In (a) an image of the in coupled light is shown, while in (b) the cout-coupling is presented. The cross sectional of the out-coupling is shown in (c). White dashed lines represent here the waveguides. Minor scattering losses are observed and emphasize the quality of the waveguides.

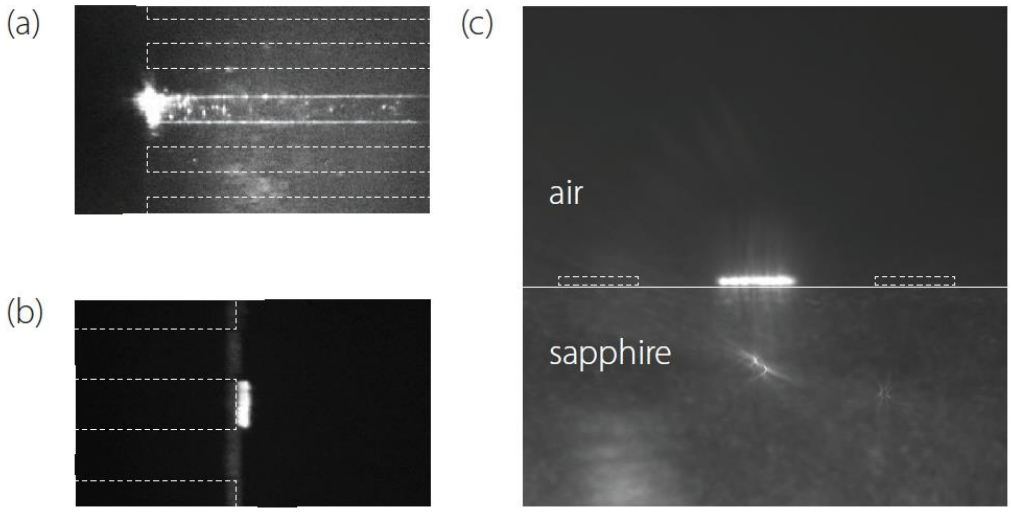

Fig. 19: In- & out-coupling by edge coupling. In (a) the in-coupling and in (b) the out-coupling of light recorded by a CCD camera above the coupling system is shown. In (c) a cross section picture of the out-coupling.

Rectangular waveguide structures were used in SHG experiments (Fig. 20). To achieve such patterning of GaN and AlN planar waveguides, a standard photolithography was process is used similar like explained for the LPS patterning. The thicknesses of such waveguides were measured using a SEM and FIB dual system. A cross-sectional trench was prepared by following procedure. First we have deposited a 1 μm thick Pt protective layer using an ion beam induced deposition with a 0.43 nA beam current. Next we have milled a cross-section using a 6.5 nA ion beam. This was followed by an 80 pA milling of the exposed cross-section, to obtain a polished surface. III-polar GaN waveguides were then investigated in order to search for modal-dispersion phase matched conditions. The thickness of the measured GaN waveguides, which was determined by FIB and SEM analysis, was around 1150 nm. Although the waveguides exhibit very smooth surface, the analysis of the image taken by CCD detector mounted above the sample, revealed that most of the light scattering takes place at the side surfaces of the waveguides. With the SEM analysis of side surfaces for waveguides with different widths, it was found out that the degree of the side roughness is especially high for waveguides with of 5 μm stripe width. For this reason measurements were done on GaN waveguides, which were at least 10 μm wide. Different lenghts of the waveguides were achieved by cleaving procedure with diamond pen, scribed straight lines perpendicular to the waveguides direction on the backside of the sapphire wafer. The lenght of theGaN waveguides used in the experiment was 1.0 mm.

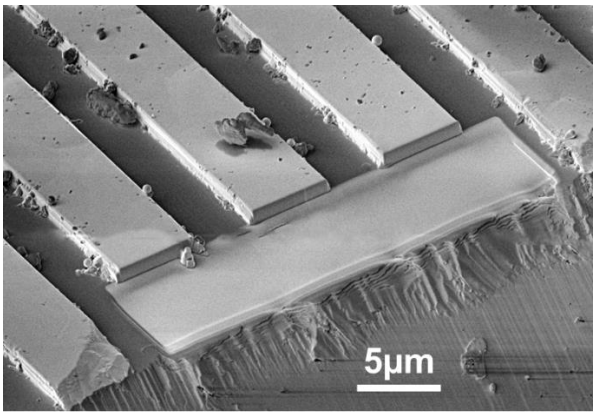

Fig. 20: Fabrication of waveguides for measurements SHG measurements. AlGaN LPS stripe waveguides can be manufactured by etching to reduce light propagation losses and to demonstrate SHG. The SEM image shows a GaN waveguide with a thickness of 0.9 µm and width of 5 µm. The front and back edges are etched by focused ion beam to achieve higher coupling efficiency.

A scan of pump wavelengths from 860 to 920 nm was performed (Ti:Sa-Laser). A clear, relatively strong peak of the SHG signal could be obtained at the wavelength of 450 nm. Measurements with different positions of the central pump wavelengths are presented in Fig 21. The maximum SHG response can be seen in Figs. 22 (g) and (h) with the central pump wavelengths of 895 and 900 nm. In order to explain the results from Fig. 22, it has been identified which fundamental mode can be phase-matched to the frequency doubled. The dispersions of the effective refractive indices for the pump and SHG waveguide modes in GaN waveguide on sapphire substrate are presented in Fig. 21. Because the effective refractive index strongly depends on the thickness of the waveguide, the values of *W* were varied within the measurement tolerances in order to check the phase matching at the pump wavelength of 900 nm. The calculations showed that the thickness of the GaN waveguide is 1140 nm, which is in good agreement with the FIB and SEM analysis of the sample. For the calculation a planar waveguide approximation is used, as the waveguides were 10 μm wide. The effective refractive indices *n*eff,*m* at different wavelengths and different waveguide thicknesses are obtained.

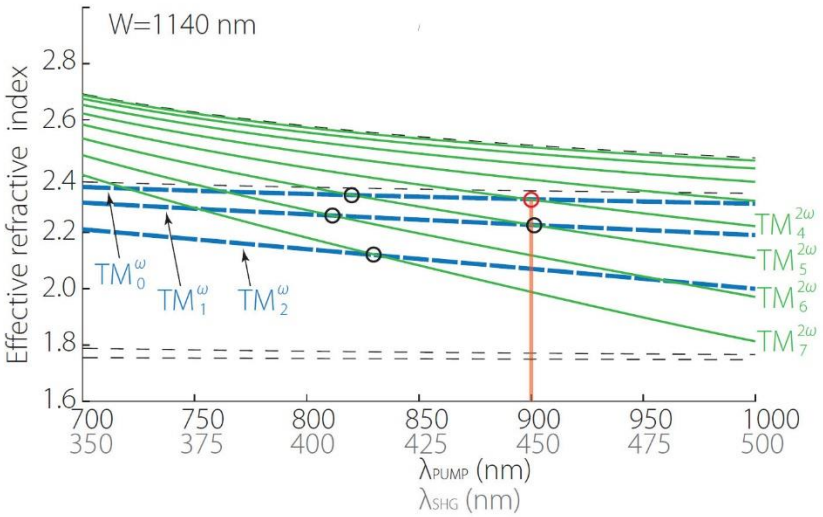

Fig. 21: The dispersions of the effective refractive index for the pump (dashed blue lines) and SHG (green lines) waveguide modes in GaN waveguides with a thickness of 1140 nm. Dashed black lines represents the dispersions of the extraordinary refractive indices of bulk GaN and sapphire at λ_P and λ_{SHG}. The red circle indicate the MDPM interaction, which is responsible for the measured SHG signal. The black circles mark other MDPM interactions, which were taken into account in overlap integral calculations.

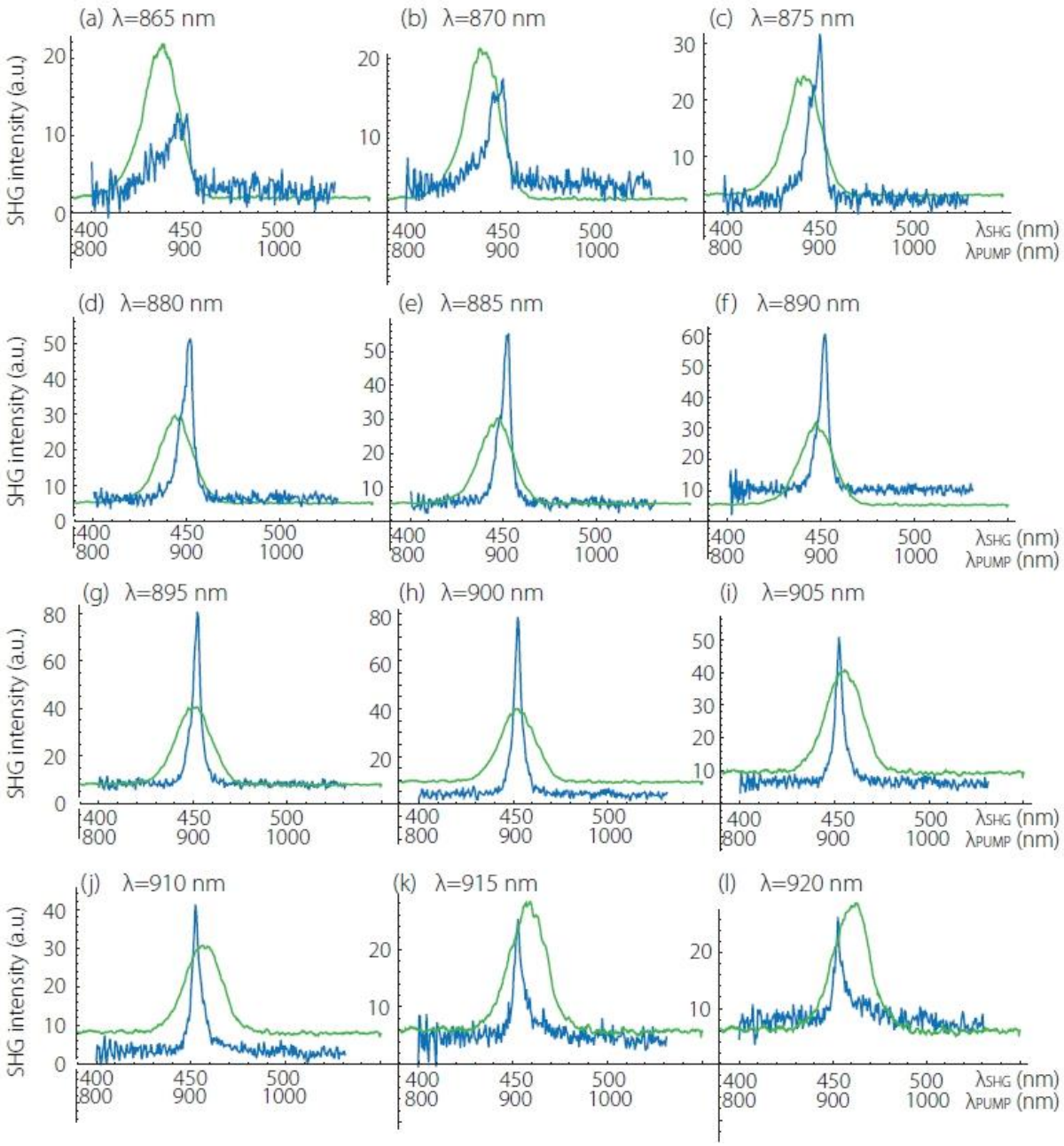

Fig. 22: Modal-dispersion phase matching SHG measurements results. The fundamental mode has been phase-matched to the frequency doubled mode. Measurements with different positions of the central pump wavelength are presented. Blue lines represent the SHG signal and the green lines represent the pump spectra. A clear and intensive peak for the SHG signal was found at 450 nm (h).

These results on modal-dispersion phase matching emphasize the capability of AlGaN LPS for SHG.

9. Summary

It was demonstrated that GaN, AlGaN and AlN lateral polar structures can be manufactured that are promising for second harmonic generation using quasi phase matching. In GaN LPS the growth rate of the polar domains significantly depends on the applied Ga supersaturation. AlN LPS can be manufactured easily with no growth rate difference between polar domains. In AlGaN LPS, it could be observed that high Ga composition in the AlxGa1-xN LPS leads to a height difference of the domains towards the III-polarity. It has been suggested that this is strongly influenced by the Ga supersaturation, as observed in GaN LPS. Nevertheless, the fabricated $Al_xGa_{1-x}N$ LPSs are promising to be used for QPM waveguides as an alter-native to achieve deep UV light-emitters. GaN and AlN waveguides can be used to realize modal-dispersion phase matching enabling SHG.

10. Publications

The following publications have been published as part of this project:

1. M. P. Hoffmann, M. Gerhold, R. Kirste, A. Rice, C.-R. Akouala, J. Q. Xie, S. Mita, R. Collazo and Z. Sitar, Proceedings of SPIE **8631**, 86311T (2013).
2. R. Kirste, S. Mita, L. Hussey, M. P. Hoffmann, W. Guo, I. Bryan, Z. Bryan, J. Tweedie, J. Xie, M. Gerhold, R. Collazo and Z. Sitar, Appl. Phys. Lett. **102** (18), 181913-181914 (2013).
3. M. Rigler, M. Zgonik, M. P. Hoffmann, R. Kirste, M. Bobea, R. Collazo, Z. Sitar, S. Mita and M. Gerhold, Appl. Phys. Lett. **102** (22), 221106-221105 (2013).
4. D. Skuridina, D. V. Dinh, B. Lacroix, P. Ruterana, M. Hoffmann, Z. Sitar, M. Pristovsek, M. Kneissl and P. Vogt, J. Appl. Phys. **114** (17), - (2013).
5. C. T. Shelton, E. Sachet, E. A. Paisley, M. P. Hoffmann, J. Rajan, R. Collazo, Z. Sitar and J.-P. Maria, J. Appl. Phys. **115** (4), - (2014).
6. R. Kirste, S. Mita, M. P. Hoffmann, L. Hussey, W. Guo, I. Bryan, Z. Bryan, J. Tweedie, M. Gerhold, A. Hoffmann, R. Collazo and Z. Sitar, Phys. Status Solidi C **11** (2), 261-264 (2014).
7. M. P. Hoffmann, Doctoral Thesis, Technische Universität Berlin, 2013.
8. M. Rigler, Doctoral Thesis, University of Ljubljana, 2014.

The following publications will be published as part of this project:

1. M. P. Hoffmann, R. Kirste, S. Mita, W. Guo, J. Tweedie, I. Bryan, Z. Bryan, M. Gerhold, R. Collazo, and Z. Sitar, "Growth and characterization of $Al_xGa_{1-x}N$ lateral polarity structures", manuscript send to Physica Status Solidi (b).
2. M. Rigler, J. Buh, M. P. Hoffmann, R. Kirste, M. Bobea, S. Mita, M. Gerhold, R. Collazo, Z. Sitar, and M. Zgonik, "Ellipsometric characterization of Al- and N-polar AlN waveguides for integrated optics", manuscript send to Applied Physics letters.
3. Rajan, R. Kirste, M. Hoffmann, W. Guo, I. Bryan, L. Hussey, M. Gerhold, S. Mohn, M. Albrecht, R. Collazo and Z. Sitar, "Controlled mass transport between Ga- and N-polar domains in GaN lateral polarity structures", Journal of Applied Physics, manuscript in preparation.